ARTICLE

Vascular Labeling of Luminescent Gold Nanorods Enables 3-D Microscopy of Mouse Intestinal Capillaries

Shiue-Cheng Tang, Ya-Yuan Fu, Wen-Fu Lo, Tzu-En Hua, and Hsing-Yu Tuan*

Department of Chemical Engineering, National Tsing Hua University, Hsinchu, Taiwan 30013

ABSTRACT In this study, we aimed to use gold nanorods (Au-NRs) as luminescent substrates for labeling of the mouse intestinal blood vessels for tissue imaging. The labeled intestine was subjected to 3-D confocal microscopy to reveal the intricate morphology of the intestinal capillaries. Using the Au-NR's unique near-infrared excitation and visible fluorescence emission, we observed low noise background compared to the tissue's high autofluorescence from blue laser excitation. We took advantage of this sharp contrast in optical properties to achieve 3-D visualization of the intestinal microstructure and vasculature with capillary-level resolution. This new optical application demonstrates the Au-NR's distinctive properties in vascular labeling and fluorescence microscopy for 3-D illustration of intestinal vasculature.

KEYWORDS: 3-D confocal microscopy · gold nanorods · intestinal vascular imaging · optical imaging · photoluminescence

Gold nanorods (Au-NRs) have recently emerged as effective luminescent particles for bioimaging.[1−6] Compared with conventional organic dyes, Au-NRs possess a highly efficient absorption at the near-infrared wavelengths, emit visible wavelength fluorescence under multiple photon excitation, and experience minimal, if any, photobleaching during laser excitation.[7,8] When applied as the fluorophores in two-photon microscopy, for instance, Au-NRs can emit bright two-photon-induced visible light due to their large two-photon action cross sections (>2000 Goeppert−Mayer units in comparison to 1−300 units for organic fluorophores) and longitudinal plasmon resonances.[9] Moreover, the long-wavelength laser excitation in two-photon imaging reduces Rayleigh scattering, thus facilitating photon penetration in biological tissues for deep-tissue microscopy.[10] However, to date, Au-NRs have only been used in planar imaging to label the cellular monolayers at tissue culture surfaces,[1,11,12] which do not have the three-dimensional (3-D) tissue structure to fully demonstrate the properties of Au-NRs in optical imaging.

In this research, we applied Au-NRs in mouse vascular labeling to reveal the 3-D capillary structure of the small intestine. We aimed to use the Au-NR-mediated near-infrared confocal microscopy to visualize the intricate morphology of the intestinal vasculature. The intestinal microvessels play a central role in nutrient absorption and immune response against infections.[13,14] In cancer development, the abnormal vascular morphology derived from angiogenesis is a trait of tumor progression.[15] Although detailed analysis of the vascular network is greatly needed in basic and clinical research, visualization of the gastrointestinal vasculature is often limited by the spatial resolution of the imaging tools.

Among the available imaging technologies, noninvasive magnetic resonance imaging (MRI) can image deep into the tissue and provide 3-D information; however, the resolution is too low to observe the vascular and capillary structure at the cellular level.[16] With respect to routine histochemical staining and microscopy, the microtome-based 2-D tissue analysis allows micrometer-level resolution but confines the view at a specific cut plane.[17] In addition, the distortions and artifacts caused by microtome slicing as well as the disconnection between sectioned tissues prevent a global view of the vascular network. To date, detailed morphologic analysis of the intestinal microcirculation depends on vascular corrosion casts. However, this method strips away the mucosa for scanning electron microscopy (SEM), thus rendering it incapable of providing an integrated visualization of the vasculature with its surrounding tissues.[15,18]

New advances in 3-D optical methods and the Au-NR-mediated vascular labeling

*Address correspondence to hytuan@che.nthu.edu.tw.

Received for review August 25, 2010 and accepted September 24, 2010.

Published online October 1, 2010.
10.1021/nn102157a

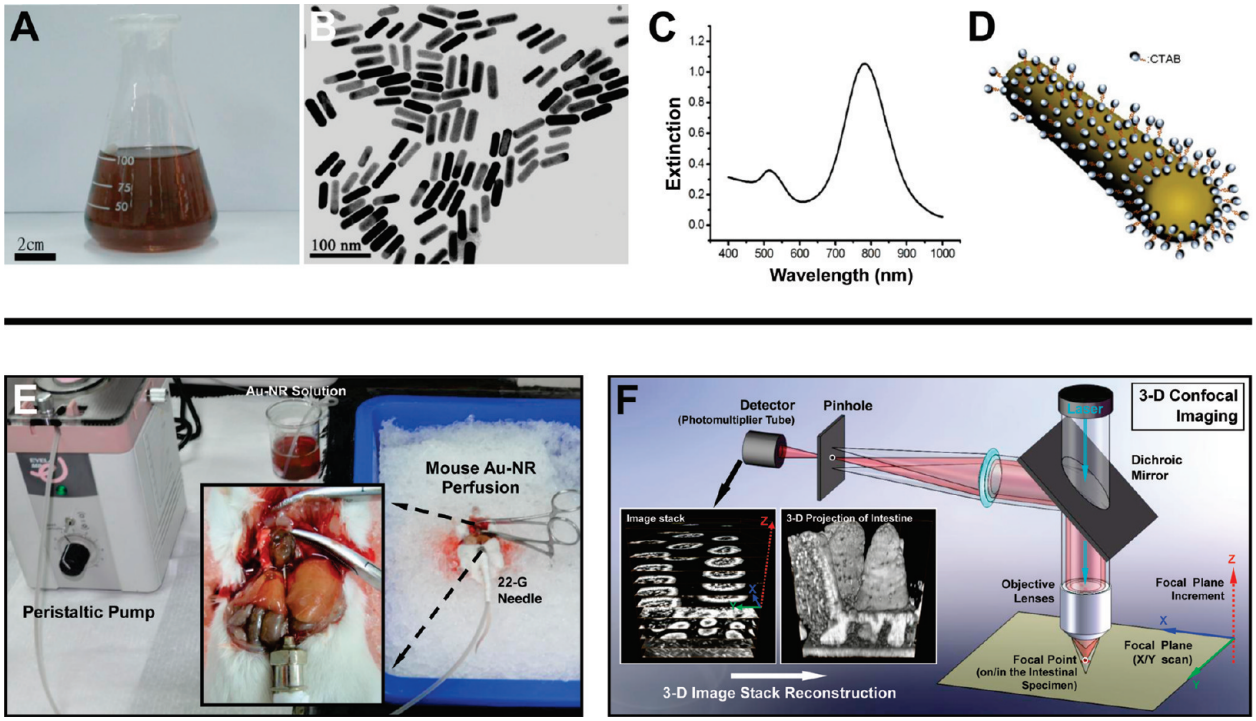

Figure 1. (A) Gross view of the dark-brown Au-NRs in the flask. (B,C) TEM image and absorption spectrum of the as-synthesized Au-NRs, showing their specific aspect ratio and the peaks of absorbance, respectively. (D) Illustration of the Au rod structure with CTAB molecules coated on the surface. (E) Transcardiac perfusion of Au-NRs into the mouse circulatory system. A needle was used to pierce the left ventricle and then enter the aorta ascendens, where it was clamped by a hemostat, to deliver Au-NRs through a peristaltic pump. (F) Schematic of 3-D confocal microscopy and image rendering of the acquired optical stack for stereoprojection of the scanned intestinal structure.

provide the tools to build the vascular diagram with the associated mucosal structure. First, the process of optical clearing—application of immersion solution to reduce random scattering as light travels across media—generates transparent intestine by minimizing refractive mismatch between the tissue constitutes (refractive index at ~1.46) and fluids (water has a lower refractive index at 1.33).[19−22] This allows direct visualization of the interior domain of the mucosa and submucosa *via* optical microscopy.[23] Second, in this research, we discovered that the perfusion (fill-in) labeling of the mouse blood vessels with Au-NRs was compatible with the optical-clearing process to generate transparent gut tissues for 3-D microscopy. Panoramas of the mouse intestinal vasculature and our use of the Au-NR labeling to facilitate 3-D capillary microscopy are presented in this report.

RESULTS AND DISCUSSION

Unlike small-area cellular labeling, mouse vascular labeling requires a substantial amount of Au-NRs for perfusion. Therefore, we devised a two-step process involving Ag(I)-assisted, seed-mediated growth of gold to produce Au-NRs at the subgram level to provide sufficient substrates for perfusion labeling.[24−26]

Figure 1A shows a representative batch of the as-synthesized, dark-brown Au-NRs. The structural and optical properties were confirmed by the transmission electron micrograph (TEM) (Figure 1B) and the absorption spectrum (Figure 1C), respectively. Specifically, the Au-NRs had an average aspect ratio of 3.8 ± 0.4 and carried a longitudinal plasmon mode centered at ~780 nm. In addition, the ratio of the peak absorbance—the intensity of the maximum longitudinal plasmon band divided by that of the maximum transverse plasmon band—was ~3, indicating a dominant population of nanorods, relative to nanospheres, in the solution. An illustration of the Au-NR crystal coated with the CTAB surfactant molecules (which were derived from the synthesis reaction) is shown in Figure 1D.

Next, we used the Au-NRs in mouse transcardiac perfusion to label of the small intestinal vasculature for tissue imaging (Figure 1E).[27,28] We specifically targeted the intestinal microstructure and vasculature for visualization, which was based on our previous experience using a microtome-free, 3-D confocal imaging method for examination of mouse intestine (Figure 1F).[23]

In addition, Figure 2A shows the serosal domain of the mouse intestine with Au-NR-labeled vasculature. The electron micrograph of the perfused blood vessel is shown in Figure 2B, in which the lumen is filled with Au-NRs and the endothelial lining is attached with the nanorods.

To visualize the Au-NR-labeled vasculature in the mouse intestine, we applied optical clearing to generate transparent specimens to promote photon penetration in the tissue. This step was essential for deep-tissue fluorescence detection of Au-NRs. It facilitated

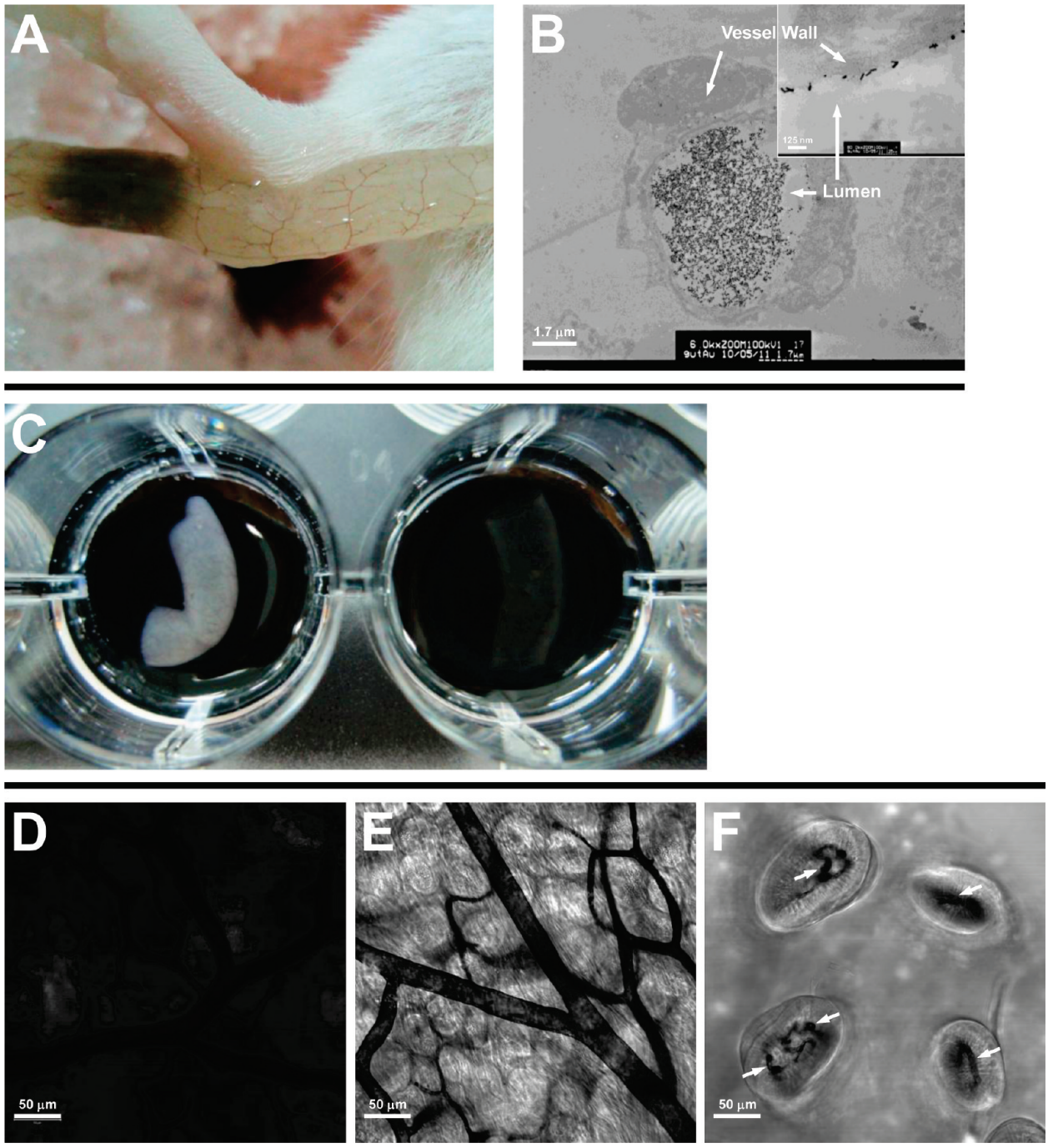

Figure 2. (A) Serosal domain of the mouse intestine with Au-NR-labeled vasculature. The vascular networks turned dark-brown (the color of Au-NRs) after the transcardiac perfusion. (B) TEM images of the perfused duodenum, revealing that the lumen of the intestinal blood vessel is filled with Au-NRs (bar = 1.7 μm) and the endothelial lining is attached with the nanorods (inset, bar = 125 nm). (C) Segments of the Au-NR-perfused duodenum immersed in saline (left, control) and the optical-clearing solution (right). Particularly, the optical-clearing immersion promoted photon penetration, rendering a transparent intestine. (D−F) Transmitted light micrographs of the Au-NR-labeled duodenal specimens immersed in saline (D, control) and the optical-clearing solution (E and F). (D,E) Serosal domain. (F) Luminal domain. The arrows in (F) indicate the labeled villus capillaries. Bar = 50 μm.

the travel of the emitted visible spectrum fluorescence (470−740 nm, induced by the 770 nm laser excitation) (optimization of the imaging parameters is shown in the Supporting Information, Figure S1) with reduced scattering in the media.[23] Figure 2C compares the gross views of the opaque and the transparent gut tissues. The transmitted light micrographs of the opaque and the optical-cleared tissues are shown in Figure 2D−F. Specifically, panels E and F of Figure 2 show the Au-NR-labeled vasculature in the serosal domain (around the crypts) and the villi, respectively.

We next used confocal microscopy to visualize the Au-NR-labeled intestinal vasculature. Figure 3 shows the cross sections of the mouse duodenum, in which the intestinal lumen as well as the villi and crypts can be seen in both sets of gross images. Specifically, Fig-

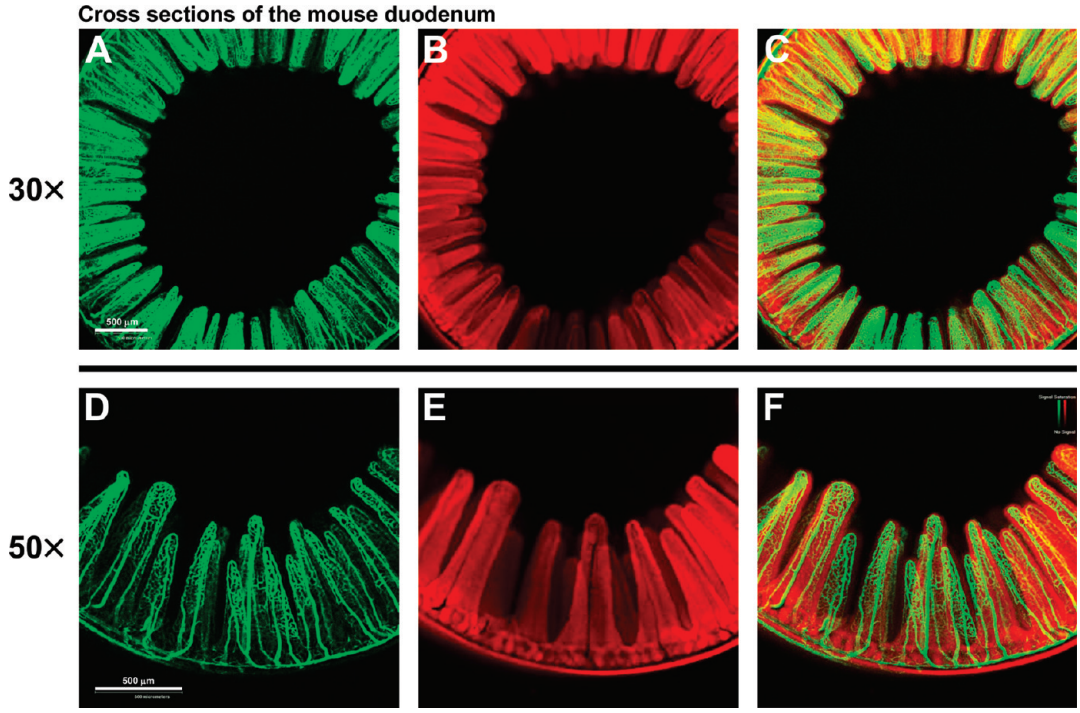

Figure 3. Gross views of the Au-NR-labeled intestinal vasculature. Cross sections of the mouse duodenum examined under 30× and 50× magnifications to reveal the Au-NR-labeled vasculature (green) and the tissue structure (red). (A,D) Duodenal vasculature revealed by Au-NRs' fluorescence. (B,E) Duodenal microstructure revealed by the tissue's autofluorescence. (C,F) Merged displays of the two signals. Bar = 500 μm.

ure 3A,D shows the fluorescent signals of the perfused Au-NRs; panels B and E show the autofluorescence from the tissue structure (excitation = 488 nm/detector's bandwidth = 493−740 nm), and panels C and F are the merged presentation of the two signals. We used Figure 3B,E as the control to demonstrate the strong, intrinsic fluorescence background from the mouse intestine when the 488 nm blue laser was used as the excitation source. By contrast, when the 770 nm near-infrared laser was used to reveal the Au-NR-labeled vasculature, we were able to avoid the autofluorescence from the intestinal tissue and generate clear signals to visualize the embedded blood vessels (Figure 3A,D).

The low noise background of the Au-NRs' fluorescence imaging can be attributed to two factors. First, biological tissues have low photon absorption at the infrared spectrum, in comparison to that at the visible spectrum, to induce the autofluorescence.[29] The intestine thus generated less autofluorescence at the 770 nm excitation to interfere with Au-NRs' signals. Second, because autofluorescence usually has longer wavelengths compared with the excitation wavelength (the Stokes shift), the unique upconversion-like photoluminescence of Au-NRs avoids the long-wavelength autofluorescence by allowing signal detection at the visible range (470−740 nm).[30,31]

Next, we zoomed in to visualize the villus microvasculature with high definition. Figure 4A−D and Video S1 (Supporting Information) present an imaging path with the focal plane (*X*/*Y* plane) in parallel with the villus-crypt axis and the focal depth following the longitudinal direction (*Z*-axis), which provided a continuous flow of information for microscopic inspection. The sharp contrast between Au-NR-labeled vasculature and the surrounding microstructure, revealed by the 770 and 488 nm excitations, respectively, provided a new approach to examine the intestinal microstructure and vasculature simultaneously. Furthermore, unlike the conventional microtome-based 2-D tissue analysis, the 3-D optical method was noninvasive to the tissue structure, thus rendering it capable of examining a region of the gut mucosa *in situ*.

By taking advantage of voxel-based confocal micrographs, we were able to digitally process the acquired image stack to present the interior as well as the surface details of the imaged tissue structures. Figure 4E shows the high-resolution, 3-D projection of the villus microstructure, derived from the image stack shown in Video S1. In order to reveal the Au-NR-labeled microvasculature in the villi, in Figure 4F, we digitally subtracted a cuboid from the scanned region (*via* the volume-editing function of Amira image reconstruction software) to expose the interior domain of the villus structure.

In addition, we created a composite image gallery by adding the orthogonal slices (Figure 4G) to the 3-D vascular projection (Figure 4H). This allowed a detailed examination of the microstructure and Au-NR-labeled vasculature in the interior domain of the scanned region. Video S2 is a continuous display of the projection gallery. The 360° panoramic presentation of Figure 4H is shown in Video S3 in the Supporting Information. The

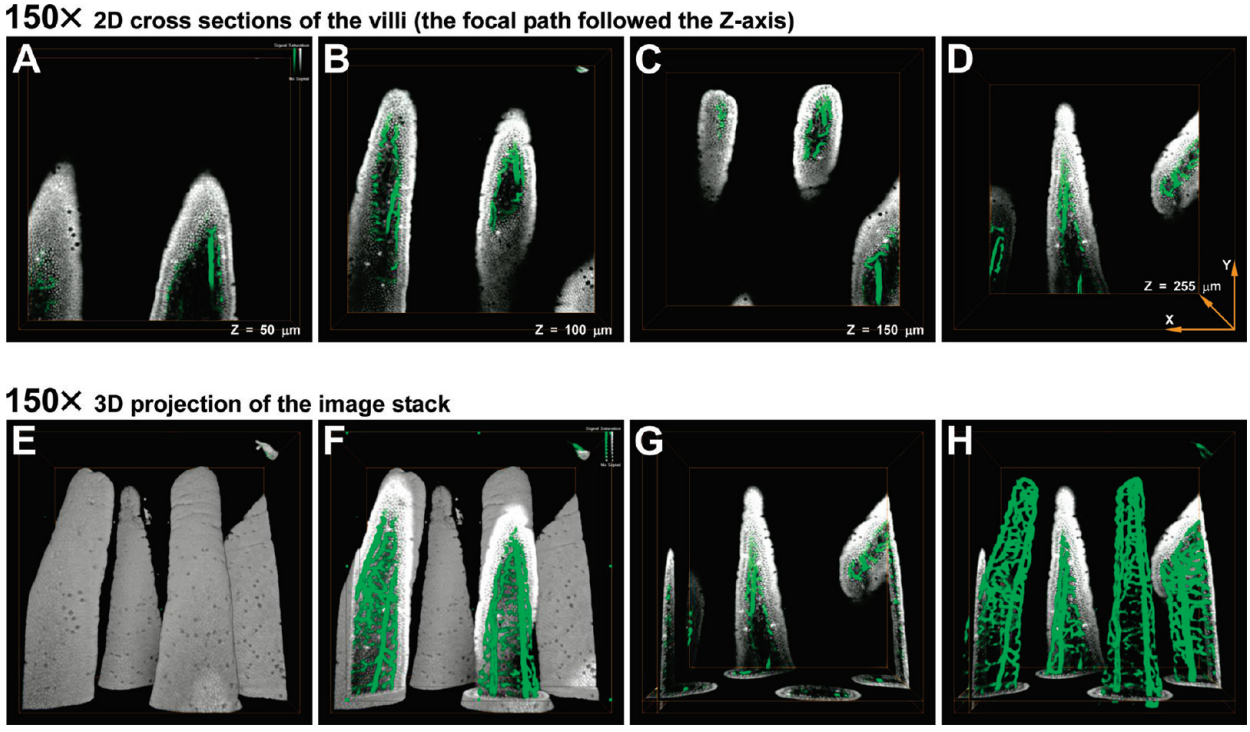

Figure 4. High-resolution, 3-D microscopy of the Au-NR-labeled villus microvasculature. (A−D) Confocal micrographs at different focal depths of the duodenal specimen reveal the villus microstructure (gray) and vasculature (green). The 2-D micrographs were projected in a 3-D box to illustrate the focal depth. The serial optical sections of the imaged region are shown in Video S1 in the Supporting Information. Dimensions of the scanned volume: 563 μm (*X*) × 563 μm (*Y*) × 255 μm (*Z*, the focal depth). (E,F) Three-dimensional projections of the villus microstructure and the Au-NR-labeled vasculature. Panel F was derived by digitally subtracting a cuboid of the autofluorescence from panel E to reveal the embedded vasculature. (G) Orthogonal view of the image stack illustrates the vasculature in the interior domain of the villi. Four planes at the *X*/*Y*, *X*/*Z*, and *Y*/*Z* (two) domains were used in the projection. (H) Merged projection of the Au-NR-labeled vasculature and the orthogonal planes shown in panel G. Video S2 in the Supporting Information provides a continuous display of panel H following the increment of the focal depth. A 360° panoramic presentation of panel H is shown in Video S3 in the Supporting Information.

additional high-resolution, 3-D projections of the duodenal microstructure and vasculature are presented in Figure S2 in the Supporting Information.

It should be noted that, in this research, the Au-NR labeling and optical clearing of the intestinal tissue (Figure 2) were performed on the deceased animals. Particularly, the process of optical clearing led to reduced light scattering, thereby improving the penetration of Au-NRs' visible fluorescence in the tissue. This allowed us to acquire higher resolution as well as 3-D images of the vascular structure in comparison to the previous work of *in vivo* imaging of Au-NRs in the blood vessels.[1] However, because the labeling, clearing, and imaging processes were all performed on the tissues of the deceased animals, or *in vitro*, the ability to carry out longitudinal examinations was limited to a single time point. By contrast, the resolution of the *in vivo* Au-NR imaging was limited due to light scattering, yet the key feature remains in that it can provide real-time as well as longitudinal imaging data.

CONCLUSION

This research demonstrated for the first time that Au-NRs can be used in 3-D microscopic tissue imaging for characterization of the mouse vasculature. We applied transcardiac perfusion of the CTAB-coated Au-NRs to label the intestinal blood vessels for fluorescence imaging. Using the unique photoluminescence of Au-NRs (near-infrared excitation and visible fluorescence emission), we imaged the intestinal vasculature by 3-D confocal microscopy with efficient fluoresce excitation and emission in the optical-cleared specimen. This imaging approach, based on Au-NRs' unique optical properties, perfusion labeling, and 3-D confocal microscopy, permits us to change our conventional planar view of the tissue structure into a 3-D panorama for better characterization of the vascular/capillary network.

METHODS

Synthesis and Characterization of Gold Nanorods. Ag(I)-assisted, seed-mediated growth of gold was applied to produce Au-NRs with a modified version.[24−26] To prepare the seed solution, the aqueous $HAuCl_4 \cdot 3H_2O$ (0.01 M, 0.25 mL) was added to the recrystallized, iodide-free hexadecylcetyltrimethylammonium bromide solution (CTAB, 0.01 M, 9.75 mL) in a water bath maintained at 30 °C. When the color of the solution appeared bright yellow-brown, an aqueous, ice-cold sodium borohydride solution ($NaBH_4$, 0.01 M, 6 mL) was slowly added for reaction. The resulting mixture was stirred vigorously and aged for 2 h to form the

gold seeds. Meanwhile, the growth solution was prepared by adding CTAB (0.10 M, 95 mL), $HAuCl_4 \cdot 3H_2O$ (0.01 M, 5 mL), and $AgNO_3$ (0.01 M, 0.95 mL) solutions sequentially into a flask with vigorous stirring. Finally, Au-NRs (~0.1 g/batch) were produced by sequential addition of ascorbic acid (0.1 M, 0.55 mL) and seed solution (0.12 mL) to the growth solution with gentle mixing for 12 h.

Absorption spectra of the solutions were taken on a U3300 Scan UV−vis−NIR spectrophotometer. TEM images were obtained with a Hitachi H-7100. The TEM grids were prepared as follows: Typically 20 mL of the solution was centrifuged for 14 min at a speed of 5000 rpm to precipitate the solid. The colorless supernatant was discarded. The solid residue was redispersed in DI water and centrifuged again. Finally, the solid residue was dispersed in a suitable volume of DI water depending on the quantity of the residue. A total of 7 μL of this solution was dropcast on the TEM grid and allowed to dry in the vacuum oven at 40 °C.

Animal. Duodena harvested from the female wild-type BALB/c mice (~20−25 g) (obtained from BioLASCO Taiwan Co, Ltd., Taipei, Taiwan) were used to acquire gross views and high-resolution images of the intestinal microstructure and vasculature. Overall, six mice were used to generate representative images. The care of the animals was consistent with Guidelines for Animal Experiments, National Tsing Hua University, Taiwan.

Preparation of Duodenal Specimens. Mouse duodena were fixed by paraformaldehyde perfusion and then labeled by Au-NR perfusion prior to being harvested for examination (the step-by-step description is provided in the Supporting Information). Once harvested, duodena were flushed with cold Hank's balanced salt solution with 0.4 mol/L *N*-acetyl-L-cysteine and then phosphate-buffered saline (PBS) to remove the luminal contents. Afterward, the tissues were fixed with paraformaldehyde (4%) for one additional hour and then permeabilized with Triton X-100 (2%) overnight. The labeled specimens were immersed in the FocusClear solution (CelExplorer, Hsinchu, Taiwan) for optical clearing before being imaged *via* confocal microscopy.

Image Acquisition. Optical imaging of the intestinal specimens was performed with a Zeiss LSM 710 confocal microscope (Carl Zeiss, Jena, Germany) equipped with objectives of 5× and 10× "Fluar" lenses to acquire gross views and 25× LD "Plan-Apochromat" glycerine immersion lenses to acquire high-resolution images. The Au-NR-labeled blood vessels were excited with a Mai Tai laser (Newport Corporation, Irvine, CA) tuned at 770 nm to induce fluorescence in the visible spectrum. In the meantime, a 488 nm argon laser was used to induce autofluorescence from the specimen to outline the tissue structure. The scanning process was operated under the "multi-track" mode with the detector bandwidths set at 470−740 and 493−740 nm to collect the signals from Au-NRs and the autofluorescence, respectively. The increment of the *Z*-axis optical section was 2.5 μm when the 25× objective lenses were used to acquire high-resolution images for 3-D projection. The micrographs were recorded with 1024 × 1024 pixels of the *X*/*Y* plane. The pixel intensity was set to be the mean of four scans, and the value ranged from 0 to 4095 (12-bit data).

The labeling of the intestinal vasculature was also examined by TEM. In this analysis, the fixed duodenal sample was first dissected into small cubes (~1 mm^3) and then subjected to serial ethanol dehydration before embedding in the Spurr's resin. The tissue blocks were sectioned with ultramicrotome (Leica EM UC6, Bannockburn, IL) to obtain ultrathin sections of ~90 nm in thickness. The sections were then stained with 1% uranyl acetate and lead citrate prior to being imaged by TEM using a Hitachi H-7500 model (Tokyo, Japan) at 100 kV.

3-D Image Processing and Projection. The Zen 2009 software (Carl Zeiss) and the Amira 4.1.2 image reconstruction software (Mercury, Chelmsford, MA) were used for the 3-D projection and analysis of the confocal micrographs. The LSM confocal image data were uploaded into the Amira software, which was operated under a Dell T5400 workstation with a Linux operation system. In Videos S1 and S2 (Supporting Information), the image stacks were displayed using the "Ortho Slice" function, and the videos were made *via* the "Movie Maker" function with the increase in display time in association with the depth of the optical section. In Figure 4E,F,H and Video S3, the "Voltex" module of Amira was used to project the image stacks. In Figure 4F, the "Volume Editing" function was used to subtract a cuboid from the scanned volume to expose the interior domain of the specimen for visualization. In Video S3, the "Camera Rotation" function was used to adjust the projection angles of the 3-D images.

Acknowledgment. This work was supported in part by grants from the National Science Council (NSC 98-3011-P-007-004 and NSC 99-2221-E-007-094 to S.-C.T. and NSC 98-2221-E-007-075 and NSC 99-2221-E-007-096 to H.-Y.T.), CGMH-NTHU Joint Research Program (CMRPG380011 to H.-Y.T.), and the 5-year Research Program in NTHU, Taiwan. We thank BRC in NTHU for technical support in confocal imaging and postrecording image processing.

Supporting Information Available: Figures of (1) optimization of the confocal imaging parameters for fluorescent detection of the Au-NR-labeled vasculature and (2) 3-D projection of the duodenal villi and their Au-NR-labeled vasculature; videos of (1) serial optical sections of the villus microstructure and the Au-NR-labeled microvasculature, (2) high-resolution, 3-D presentation of the Au-NR-labeled villus microvasculature, and (3) high-resolution, 360° panoramic presentation of the Au-NR-labeled villus microvasculature, and methods of vascular labeling and fixation *via* transcardiac perfusion. This material is available free of charge *via* the Internet at http://pubs.acs.org.

REFERENCES AND NOTES

1. Wang, H. F.; Huff, T. B.; Zweifel, D. A.; He, W.; Low, P. S.; Wei, A.; Cheng, J. X. *In Vitro* and *In Vivo* Two-Photon Luminescence Imaging of Single Gold nanorods. *Proc. Natl. Acad. Sci. U.S.A.* **2005**, *102*, 15752–15756.
2. Sonnichsen, C.; Alivisatos, A. P. Gold Nanorods as Novel Nonbleaching Plasmon-Based Orientation Sensors for Polarized Single-Particle Microscopy. *Nano Lett.* **2005**, *5*, 301–304.
3. Tong, L.; Wei, Q. S.; Wei, A.; Cheng, J. X. Gold Nanorods as Contrast Agents for Biological Imaging: Optical Properties, Surface Conjugation and Photothermal Effects. *Photochem. Photobiol.* **2009**, *85*, 21–32.
4. Huang, X. H.; Neretina, S.; El-Sayed, M. A. Gold Nanorods: From Synthesis and Properties to Biological and Biomedical Applications. *Adv. Mater.* **2009**, *21*, 4880–4910.
5. Tabor, C.; Haute, D. V.; El-Sayed, M. A. Effect of Orientation on Plasmonic Coupling between Gold Nanorods. *ACS Nano* **2009**, *3*, 3670–3678.
6. Mayer, K. M.; Lee, S.; Liao, H.; Rostro, B. C.; Fuentes, A.; Scully, P. T.; Nehl, C. L.; Hafner, J. H. A Label-Free Immunoassay Based Upon Localized Surface Plasmon Resonance of Gold Nanorods. *ACS Nano* **2008**, *2*, 687–692.
7. Mohamed, M. B.; Volkov, V.; Link, S.; El-Sayed, M. A. The 'Lightning' Gold Nanorods: Fluorescence Enhancement of over a Million Compared to the Gold Metal. *Chem. Phys. Lett.* **2000**, *317*, 517–523.
8. Imura, K.; Nagahara, T.; Okamoto, H. Near-Field Two-Photon-Induced Photoluminescence from Single Gold Nanorods and Imaging of Plasmon Modes. *J. Phys. Chem. B* **2005**, *109*, 13214–13220.
9. Zipfel, W. R.; Williams, R. M.; Webb, W. W. Nonlinear Magic: Multiphoton Microscopy in the Biosciences. *Nat. Biotechnol.* **2003**, *21*, 1369–1377.
10. Helmchen, F.; Denk, W. Deep Tissue Two-Photon Microscopy. *Nat. Methods* **2005**, *2*, 932–940.
11. Durr, N. J.; Larson, T.; Smith, D. K.; Korgel, B. A.; Sokolov, K.; Ben-Yakar, A. Two-Photon Luminescence Imaging of Cancer Cells Using Molecularly Targeted Gold Nanorods. *Nano Lett.* **2007**, *7*, 941–945.
12. Tong, L.; Zhao, Y.; Huff, T. B.; Hansen, M. N.; Wei, A.; Cheng, J. X. Gold Nanorods Mediate Tumor Cell Death by Compromising Membrane Integrity. *Adv. Mater.* **2007**, *19*, 3136–3141.
13. Pappenheimer, J. R.; Michel, C. C. Role of Villus Microcirculation in Intestinal Absorption of Glucose: Coupling of Epithelial with Endothelial Transport. *J. Physiol. London* **2003**, *553*, 561–574.

14. Deban, L.; Correale, C.; Vetrano, S.; Malesci, A.; Danese, S. Multiple Pathogenic Roles of Microvasculature in Inflammatory Bowel Disease: A Jack of All Trades. *Am. J. Pathol.* **2008**, *172*, 1457–1466.
15. Folarin, A. A.; Konerding, M. A.; Timonen, J.; Nagl, S.; Pedley, R. B. Three-Dimensional Analysis of Tumour Vascular Corrosion Casts Using Stereoimaging and Micro-computed Tomography. Microvascular Research. *Microvasc. Res.* **2010**, *80*, 89–98.
16. Virostko, J.; Powers, A. C. Molecular Imaging of the Pancreas in Small Animal Models. *Gastroenterology* **2009**, *136*, 407–409.
17. Wu, M. L. C.; Varga, V. S.; Kamaras, V.; Ficsor, L.; Tagscherer, A.; Tulassay, Z.; Molnar, B. Three-Dimensional Virtual Microscopy of Colorectal Biopsies. *Arch. Pathol. Lab. Med.* **2005**, *129*, 507–510.
18. Lametschwandtner, A.; Lametschwandtner, U.; Weiger, T. Scanning Electron-Microscopy of Vascular Corrosion Casts - Technique and Applications - Updated Review. *Scanning Microsc.* **1990**, *4*, 889–941.
19. Fu, Y. Y.; Tang, S. C. At the Movies: 3-Dimensional Technology and Gastrointestinal Histology. *Gastroenterology* 2010. doi:, 10.1053/j.gastro.2010.08.025.
20. Tuchin, V. V.; Wang, R. K.; Yeh, A. T. Optical Clearing of Tissues and Cells. *J. Biomed. Opt.* **2008**, *13*, 021101.
21. Tseng, S. J.; Lee, Y. H.; Chen, Z. H.; Lin, H. H.; Lin, C. Y.; Tang, S. C. Integration of Optical Clearing and Optical Sectioning Microscopy for Three-Dimensional Imaging of Natural Biomaterial Scaffolds in thin Sections. *J. Biomed. Opt.* **2009**, *14*, 044004.
22. Fu, Y. Y.; Tang, S. C. Optical Clearing Facilitates Integrated 3D Visualization of Mouse Ileal Microstructure and Vascular Network with High Definition. *Microvasc. Res.* 2010. doi:, 10.1016/j.mvr.2010.06.003.
23. Fu, Y. Y.; Lin, C. W.; Enikolopov, G.; Sibley, E.; Chiang, A. S.; Tang, S. C. Microtome-Free 3-Dimensional Confocal Imaging Method for Visualization of Mouse Intestine with Subcellular-Level Resolution. *Gastroenterology* **2009**, *137*, 453–465.
24. Gou, L. F.; Murphy, C. J. Fine-Tuning the Shape of Gold Nanorods. *Chem. Mater.* **2005**, *17*, 3668–3672.
25. Smith, D. K.; Korgel, B. A. The Importance of the CTAB Surfactant on the Colloidal Seed-Mediated Synthesis of Gold Nanorods. *Langmuir* **2008**, *24*, 644–649.
26. Millstone, J. E.; Wei, W.; Jones, M. R.; Yoo, H. J.; Mirkin, C. A. Iodide Ions Control Seed-Mediated Growth of Anisotropic Gold Nanoparticles. *Nano Lett.* **2008**, *8*, 2526–2529.
27. Ravnic, D. J.; Jiang, X.; Wolloscheck, T.; Pratt, J. P.; Huss, H.; Mentzer, S. J.; Konerding, M. A. Vessel Painting of the Microcirculation Using Fluorescent Lipophilic Tracers. *Microvasc. Res.* **2005**, *70*, 90–96.
28. Li, Y.; Song, Y.; Zhao, L.; Gaidosh, G.; Laties, A. M.; Wen, R. Direct Labeling and Visualization of Blood Vessels with Lipophilic Carbocyanine Dye DiI. *Nat. Protoc.* **2008**, *3*, 1703–1708.
29. Lichtman, J. W.; Conchello, J. A. Fluorescence Microscopy. *Nat. Methods* **2005**, *2*, 910–919.
30. Wang, H. Q.; Nann, T. Monodisperse Upconverting Nanocrystals by Microwave-Assisted Synthesis. *ACS Nano* **2009**, *3*, 3804–3808.
31. Nguyen, T. D.; Dinh, C. T.; Do, T. O. Shape- and Size-Controlled Synthesis of Monoclinic ErOOH and Cubic Er_2O_3 from Micro-to-Nanostructures and Their Upconversion Luminescence. *ACS Nano* **2010**, *4*, 2263–2273.